Research Article

Xiaofang Zou, Tian Zhu, Jiangquan Tang, Weixing Gan*, and Guangzai Nong*

Doping silver nanoparticles into reverse osmosis membranes for antibacterial properties

https://doi.org/10.1515/epoly-2022-8087
received October 07, 2022; accepted December 22, 2022

Abstract: Polyamide composite reverse osmosis (RO) membranes occupy an important position in water treatment. However, membrane fouling, especially biofouling, can lead to a significant decrease in membrane permeability. Therefore, reducing biological contamination is a significant and important property of an RO membrane. In this article, a hypothesis on the development of a new kind of RO membrane for antibacterial purposes was prepared by the modification of gallic acid (GA) and silver nanoparticles (AgNPs). Then, experiments were carried out to verify the hypothesis, getting a modified RO membrane with the composite of GA@AgNPs. The water flux of the GA@AgNPs RO membrane was 31.1 $L \cdot m^{-2} \cdot h^{-1}$, which was 46.7% higher than that of the original membrane, while the rejection rate of salt remained at 93.8–97.6%. Moreover, the GA@AgNPs RO membranes exhibited outstanding antibacterial properties with more than 99.9% antibacterial efficiency against both *Escherichia coli* and *Staphylococcus aureus*. Our work provides a new idea for solving the problem of biofouling RO membranes.

Keywords: reverse osmosis membranes, biofouling, antibacterial, water flux, the rejection rate

1 Introduction

The current global shortage of freshwater resources has affected the sustainable development of human beings (1). Therefore, seawater and some wastewater were treated by evaporation and reverse osmosis (RO) membrane technology to obtain enough freshwater for life and industrial manufacturing (2). Polyamide RO composite membranes are usually formed by the interfacial polymerization of *m*-phenylenediamine (MPD) in the water solution and trimesoyl chloride (TMC) in the organic solution on the polysulfone (PSF) support layer, and the preparation method is simple and feasible. In the application of RO membrane technology, polyamide RO membranes occupy a dominant position in the RO membrane market due to their advances in higher salt rejection, a longer working life, and a wider field of application. However, polyamide RO membranes are naturally prone to fouling, which seriously affects their working efficiency and becomes a major obstacle to their popularization and application (1).

Polyamide RO membrane fouling is caused by many reasons, among which biofouling is the main reason. Severe biofouling can lead to a significant loss of water permeability and thereby reduce the mass and quality of the generated freshwater (3,4). To reduce biofouling, physical and chemical pretreatments and water disinfection are always applied to prevent biofouling (5). However, the water treated by those methods still contained a small number of microorganisms, which should grow and reproduce continuously on the membrane surface, and also lead to membrane fouling (6). Therefore, besides the general pretreatments, it is significantly important for the preparation of a polyamide RO membrane with the property of being antibacterial for reducing biofouling.

To obtain an antibacterial polyamide RO membrane, modification methods such as surface modification and various nano-doping have been developed (6). In particular, silver nanoparticles (AgNPs), as a nanomaterial with strong antibacterial properties, has attracted more and more attention from researchers (7). However, AgNPs have poor dispersibility; hence, directly introducing AgNPs into a polyamide composite membrane should cause an aggregation, which makes it difficult to form a complete selective layer to fully connect to the bacteria for their death (8,9).

In order to solve the problem of AgNPs aggregation, researchers developed preparation methods such as

* **Corresponding author: Weixing Gan,** School of Resources, Environment and Materials, Guangxi University, Nanning, 530004, Guangxi, China, e-mail: gwxgxdx@126.com
* **Corresponding author: Guangzai Nong,** School of Resources, Environment and Materials, Guangxi University, Nanning, 530004, Guangxi, China, e-mail: gz.nonginguilin@163.com
Xiaofang Zou, Jiangquan Tang: School of Resources, Environment and Materials, Guangxi University, Nanning, 530004, Guangxi, China
Tian Zhu: School of Light Industry and Food Engineering, Guangxi University, Nanning, 530004, Guangxi, China

physical adsorption, layer-by-layer coating, and *in situ* incorporation. For instance, Yin et al. reported that the grafting of AgNPs to a thin-film composite membrane surface by using a bridging chemical reagent (cysteine) is easily contaminated to form covalent bonds with AgNPs (10). Ben-Sasson et al. prepared uniformly covered AgNPs on a polyamide RO membrane by reducing silver ions in solution (11). Yang et al. functionalized with poly(3-sulfopropyl methacrylate potassium salt) via atom transfer radical polymerization followed by *in situ* immobilization of AgNPs using a strong reducing agent (12). Although those methods can avoid the agglomeration of AgNPs, they require some strong reducing agents or bridging reagents, and those applied agents and bridging agents present high costs and might cause environmental pollution.

Therefore, it is necessary to develop a new method to prepare an RO membrane with antibacterial AgNPs to reduce membrane fouling. Gallic acid (GA) is a natural polyphenol in plants, such as legumes, vegetables, fruits, and beverages, which can act as a stabilizer for nanoparticles (13,14). As a hypothesis, GA and AgNPs–modified RO membrane (GA@AgNPs RO) was prepared with GA as the stabilizer for AgNPs and MPD as the reducing agent. The results show that this new method enables the uniform distribution of AgNPs in the GA units connected to the polyamide layer. As a result, the modified polyamide RO membrane has a strong ability to resist biofouling.

Our strategy was designed based on the multi-functional capability of MPD. MPD monomers containing primary amine groups, which are used to form the main polyamide network, can also act as a reducing agent to produce AgNPs. We applied GA@AgNPs to RO membranes to prepare RO membranes with uniformly dispersed AgNPs. This research contributes to the theory and practice of antibacterial RO membrane preparation, which is beneficial for freshwater production and environmental protection.

2 Materials and methods

2.1 Materials and reagents

The PSF ultrafiltration membrane with a molecular weight cutoff of 20,000 Da was provided by Zhongke Ruiyang Membrane Technology (Beijing) Co., Ltd. GA, camphorsulfonic acid (CAS), MPD, and 1,3,5-benzenetricarbonyl chloride (TMC) were obtained from Shanghai McLean Biochemical Technology Co., Ltd. $AgNO_3$ ($AgNO_3$) was provided by Tianjin Obokai Chemical Co., Ltd. Triethylamine (TEA) and sodium chloride (NaCl) were provided by Tianjin Damao Chemical Reagent Factory. n-Hexane was provided by Tianjin Aopusheng Chemical Co., Ltd. *Escherichia coli* and *Staphylococcus aureus* were used for the antibacterial experiments and were provided by Guangdong Huankai Microbial Technology Co., Ltd. All solvents and reagents were of analytical grade.

2.2 Preparation of the antibacterial membrane

The GA@AgNPs RO membrane was prepared by interfacial polymerization in five steps, as shown in Figure 1.

1. Cleaning the fine pores on the surface of a PSF membrane. A PSF basement membrane was immersed in

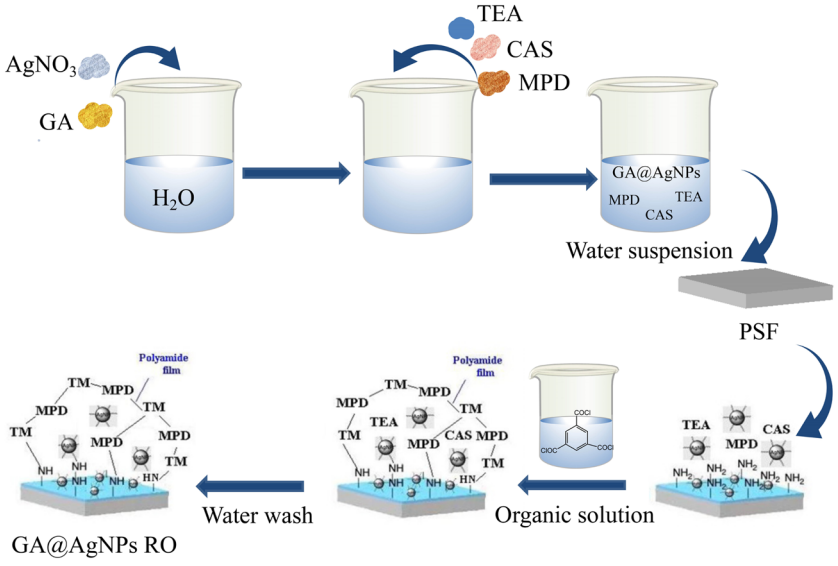

Figure 1: The process of preparation of the antibacterial RO membrane.

absolute ethanol and deionized water for 24 h to clean its fine pores, respectively.
2. Generation of a compound of AgGA. A total of 20 mL of a 0.2% $AgNO_3$ water solution was mixed with 20 mL of 0.5% of GA water solution. Therefore, a reaction occurs to generate their AgGA salt, which results in a uniform dispersion of silver ions in the GA molecules.
3. Preparation of a mixed water solution. A total of 20 mL of 2.0 wt% MPD, 20 mL of 2.2% CAS, and 20 mL of 1.3% triethylamine were mixed evenly to generate a mixed water solution.
4. Generation of a composition of AgNPs with GA. The generated compound of AgGA was added to the mixed water solution mentioned earlier. AgNPs were generated by the reducing reaction between MPD and the compound of AgGA. At the same time, the generated AgNPs were kept coordinated by the hydroxyl groups of GA, expressed as GA@AgNPs. Hence, AgNPs are uniformly dispersed.
5. Preparation of GA@AgNPs RO membrane. The cleaned PSF membrane surface was soaked in the above suspension containing GA@AgNPs for 5 min, and the excess suspension was removed. Then, 20 mL of 0.1 wt% TMC organic solution was poured onto the soaked PSF membrane surface. The excess organic solution was removed after 80 s of the reaction. The composite RO membrane was dried in an oven at 60°C for 10 min. Therefore, a composite RO membrane was prepared completely, which was mainly composed of a polyamide membrane containing the composition of GA@AgNPs, expressed as (GA@AgNPs RO).

2.3 Characterization

2.3.1 Transmission electron microscope (TEM)

The AgNPs prepared in the experimental Step 4 were washed and dried to obtain clean AgNPs. To characterize the size and morphology of AgNPs, samples were prepared by drying a drop of AgNPs suspension in ethanol in a darkroom on a 230-mesh amorphous carbon-coated copper grid and analyzed under a TEM (JEOL F200, Japan) with a lanthanum hexaboride electron gun operating at 120 kV.

2.3.2 X-ray diffraction (XRD)

The AgNPs powder samples were characterized by XRD. Among them, the radiation source used was Cu Kα (α = 1.54178 Å), the tube voltage was 40 kV, the tube current was 40 mA, the scanning range was 2θ = 10–80°, and the measurement was performed at a speed of $2°\cdot min^{-1}$.

2.3.3 Scanning electron microscopy (SEM)

SEM was used to observe the surface structure of the membrane material. First, the prepared membrane was completely dried in a vacuum drying oven at 60°C for 6 h. Then, the membrane was cut into an area of 0.25 cm^2 as the test sample. The scanning voltage was set to 10 kV, and the magnification range was 1,000 times to 60,000 times.

2.3.4 Atomic force microscopy (AFM)

AFM was used to quantitatively characterize the roughness of the membrane material. As a test sample, a dry membrane was cut into each 1 cm^2 and fixed on the sample stage with double-sided tape before being analyzed by an AFM in the range of 20 μm × 20 μm.

2.3.5 Energy dispersive X-ray spectrometer (EDX)

EDX was used to characterize the elements contained in the sample of the modified membrane.

2.3.6 Fourier transform infrared spectroscopy (FTIR)

FTIR was used to measure the infrared absorption peaks of functional groups on the surface of membrane materials. The dry membrane was cut into an appropriate size and placed directly into the sample table for a test by the wavelength of 400–6,000 cm^{-1}.

2.3.7 X-ray photoelectron spectroscopy (XPS)

XPS was used to characterize the constituent elements and characteristic element valence that stayed on the surface of the membrane material. The membrane material was thoroughly scanned in the energy range of 0–1,350 eV. Then, the energy range of the main elements of the membrane material was scanned in high resolution. Avantage software was used to perform peak-fitting processing on the data of the characteristic peaks of the Ag element. The valence information of the Ag element in the membrane material was analyzed.

2.3.8 UV-Vis diffuse reflectance spectrometer (UV-Vis DRS)

The UV-3600Plus ultraviolet-visible diffuse reflectance spectrometer produced by Shimadzu Corporation was used to conduct ultraviolet diffuse reflectance spectroscopic analysis on the RO membrane to explore the stability of the membrane. In the test, $BaSO_4$ was used as a reference, the integrating sphere was used as a carrier, the slit width of the instrument was set to 600 nm·min^{-1}, and the absorbance of the sample in the wavelength range of 200–800 nm was measured.

2.4 Separation performance testing

The separation performance of the RO membrane was tested by a cross-flow RO membrane device, as shown in Figure 2. The raw water was the sodium chloride sample with a mass concentration of 2,000 mg·L^{-1} and a pH of 7.5 ± 0.5. The membrane samples were installed in the membrane tank and operated at 1.5 MPa for 30 min to achieve a stable flux. The water flux (J, L·m^{-2}·h^{-1}) and desalinization rate (R, %) were calculated as shown in Eqs. 1 and 2, respectively:

$$J = \frac{V}{At} \tag{1}$$

$$R = 1 - \frac{C_p}{C_f} \times 100\% \tag{2}$$

where V was the volume of the permeate (L); A was the effective membrane area of the membrane (2.827×10^{-3} m^2); t was the permeation time (h); C_p and C_f are the conductivity of the permeate and the raw material, respectively (μs·cm^{-1}).

2.5 Antibacterial experiment

In this study, the antimicrobial properties of the membranes were evaluated with two types of bacteria (*E. coli* and *S. aureus*). The membrane sample was cut into a rectangle of 7.6 cm × 2.5 cm (the same size as the glass slide). The membrane, slide, and petri dish were sterilized by UV light irradiation for 2 h. Then, an alcohol lamp was lit on an ultra-clean workbench. The following procedures were performed in a sterile environment: 100 μL of bacterial suspension was evenly dispersed, with a bacterial concentration of about 1.0×10^7 cfu·mL^{-1} *E. coli* and *S. aureus* on the surface of the membrane. The membrane was lightly covered with a glass slide to ensure that the bacterial solution is evenly dispersed and not volatile. Seal the slide-covered membrane in a sterile Petri dish and place it in a constant temperature incubator at 37°C for 2 h. The membrane and slide were taken out and put into a centrifuge tube containing 20 mL of sterile normal saline and shaken well to ensure that the bacteria on the membrane and slide were completely flushed into the physiological saline. A 100 μL of the well-mixed rinse solution was taken and evenly spread on a sterile, LB solid

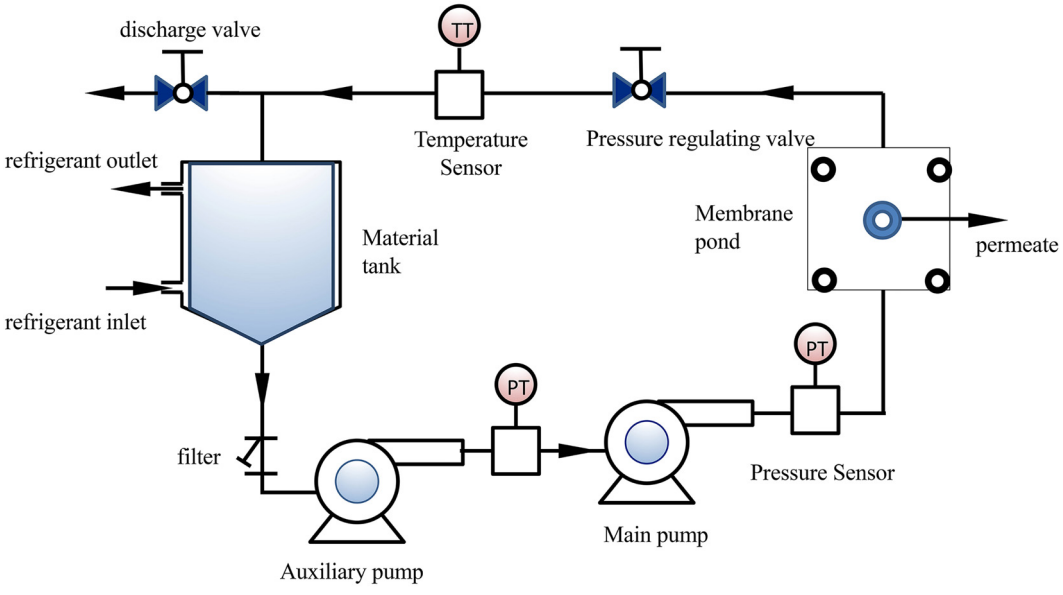

Figure 2: Flow chart of the test device for the permeability of the generated RO membrane.

medium. After culturing in a constant temperature incubator at 37°C for 24 h, record the number of colonies on the medium (A).

Blank control group: a 1.0×10^7-cfu·mL^{-1} bacterial suspension that was not in contact with the membrane was placed in a constant temperature incubator at 37°C for 2 h. Then, a 100 µL of bacterial suspension was taken and dissolved in 20 mL of sterile saline and shaken well to mix well. A 100 µL of the diluted solution, mixed evenly, was taken and spread on a sterile LB solid medium. After culturing in a constant temperature incubator at 37°C for 24 h, record the number of colonies on the solid medium (B). The bactericidal performance of the RO membrane is characterized by the bacterial mortality rate (M), which can be calculated as follows:

$$M = \frac{B - A}{B} \times 100\% \quad (3)$$

where A was the number of colonies eluted when the bacterial suspension was in contact with the membrane surface for 2 h and B was the number of colonies obtained when the bacterial suspension was in contact without the membrane surface for 2 h (blank control group).

3 Results

3.1 Characterization of AgNPs

3.1.1 Morphology and particle size analysis of AgNPs

The surface properties of AgNPs were analyzed using the TEM technique. Figure 3a and b depicts the TEM images (a) and particle size distribution images (b) of AgNPs. Figure 3a shows that the AgNPs are spherical with a layer of coating on the outside. This indicated that AgNPs were coated with GA to form GA@AgNPs particles. Furthermore, the AgNPs show a well-resolved, (111) lattice fringe (d = 0.235 nm), face-centered cubic structure, implying that the AgNPs are face-centered cubic metallic silver. Figure 3b is the size distribution histogram of AgNPs analyzed from the TEM images. As shown in Figure 3b, the particle size distribution of AgNPs ranged from 6.7 to 30.4 nm, with an average particle size of 15.1 nm.

3.1.2 Results of XRD analysis

The structural properties of AgNPs were analyzed using the XRD technique. As shown in Figure 4, the XRD

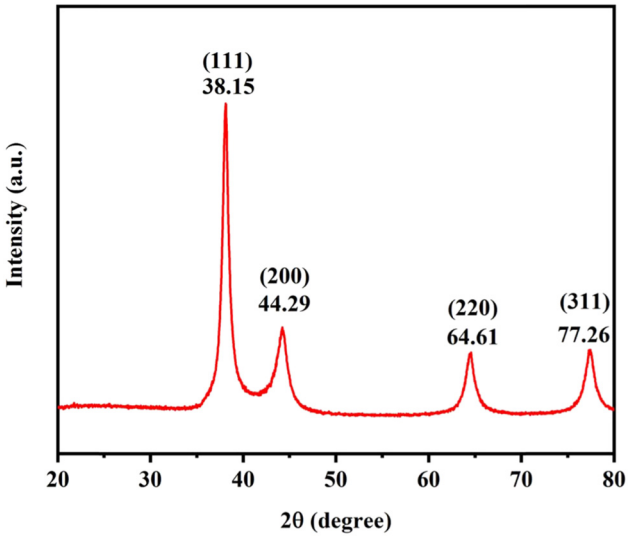

Figure 4: XRD patterns of AgNPs.

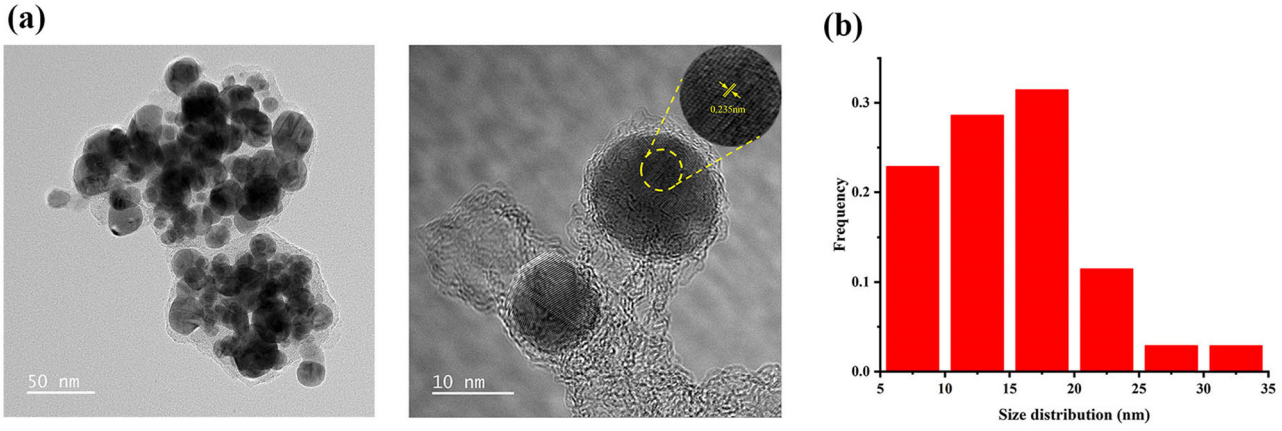

Figure 3: HRTEM images of AgNPs (a) and size distribution histograms (b).

spectrum of AgNPs has absorption peaks at 38.15°, 44.29°, 64.61°, and 77.26°, which is consistent with the data on JCPDS card 04-0783 (38.096°, 44.257°, 64.406°, and 77.452°) are basically consistent, corresponding to (111), (200), (220), and (311) crystal planes of cubic silver, respectively, indicating that the product is pure-phase elemental silver of a face-centered cubic system. The four absorption peaks of this curve are more obvious and sharp, which shows that the prepared AgNPs have good crystallinity. The size of AgNPs is estimated to be 9.8 nm from the full width at the half maximum of the (111) reflection according to the Debye–Scherrer formula. The size is slightly smaller than the average particle diameter measured by TEM images. This is because the AgNPs on the TEM have a coating layer, resulting in a larger measured size than the actual size.

3.2 The structure of the generated GA@AgNPs RO membrane

3.2.1 Morphology of the generated membrane surface

Figure 5a and b shows the SEM and AFM images of the GA@AgNPs RO membrane. As a comparison, Figure 5c and d shows the SEM and AFM images of the original RO membrane prepared only by the polyamide.

As shown in Figure 5a and b, there were many raised structures on the surface of the GA@AgNPs RO membrane. Most of these raised structures are densely distributed closed rings. By comparison, the sizes of the raised structures on the surface of the GA@AgNPs RO membrane were smaller than those of the original RO membrane prepared only by polyamide. However, the number of the raised structures increased significantly, as shown in Figure 5c and d. Therefore, the total passed surface and surface roughness of the membrane were significantly increased, leading to an increase in permeability (15).

3.2.2 Element distribution on the membrane surface

An energy dispersive spectroscopy (EDS) technique was applied to investigate the dispersibility of the AgNPs and other elements in the generated membrane. The EDS image of the GA@AgNPs RO membrane is shown in Figure 6.

As shown in Figure 6, the distribution of the Ag element is uniform. Therefore, it indicated that the AgNPs

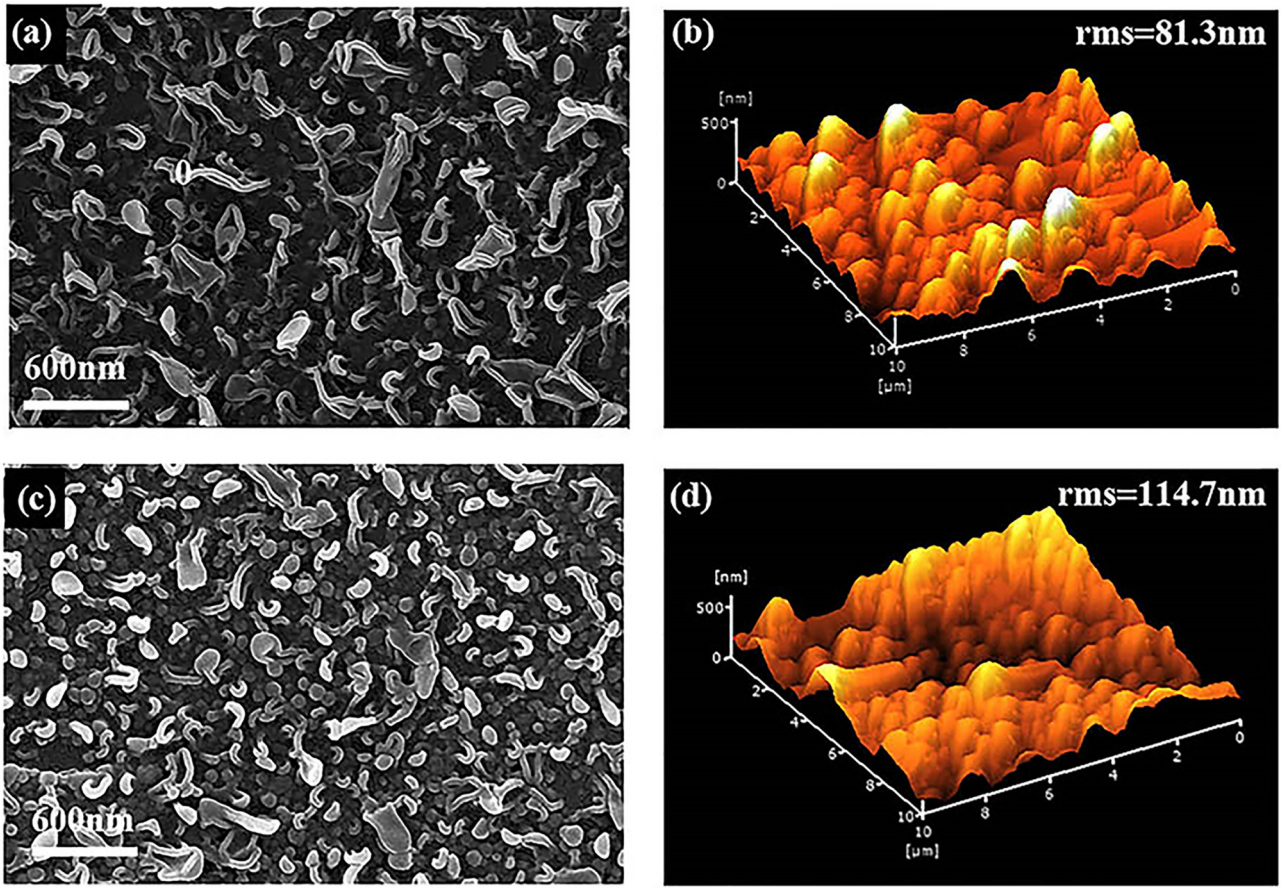

Figure 5: SEM and AFM images of the generated RO membrane compared with the original RO membrane.

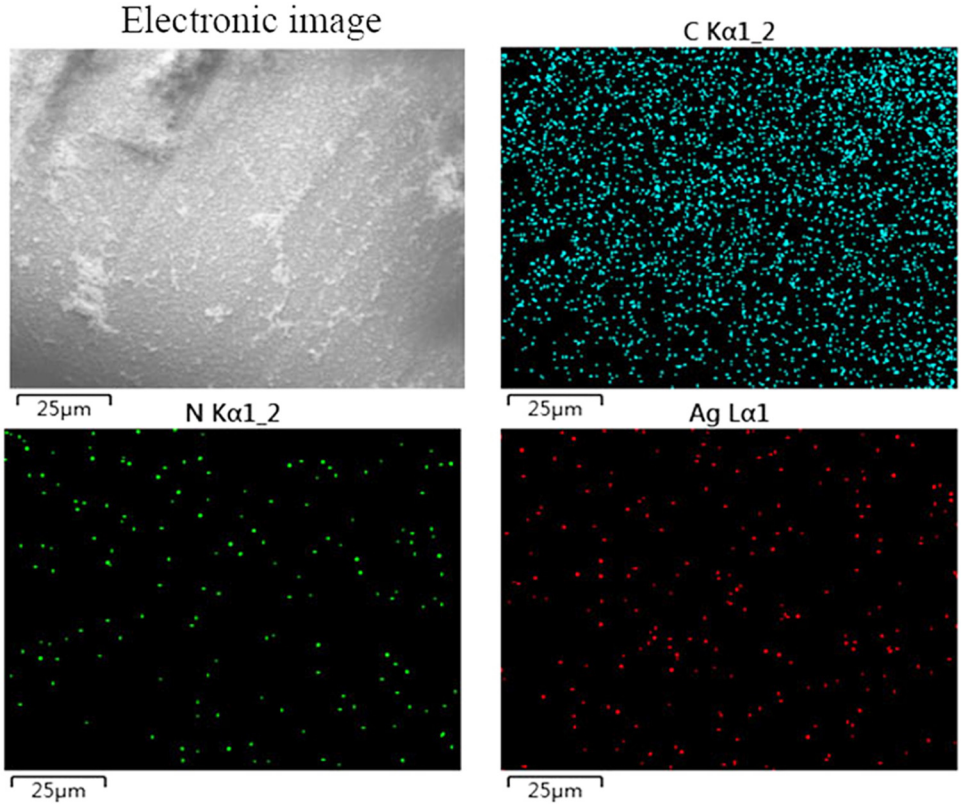

Figure 6: EDS image of the GA@AgNPs RO membrane.

were uniformly distributed on the membrane. In addition, the other elements of C, N, and O were uniformly distributed on the membrane, which means that the compositions of GA and MDP were mixed evenly in the membrane, where the AgNPs were encapsulated in the polyamide network. This is beneficial to the stable existence of AgNPs in the GA@AgNPs RO membrane.

3.2.3 Results of FTIR analysis

The FTIR spectra of the PSF membrane (blue curve), the original RO membrane by polyamide (red curve), and the GA@AgNPs RO membrane (black curve) are shown in Figure 7.

The special peaks in the spectra of the GA@AgNPs RO membrane were identified by comparison with the spectra of the PSF membrane and the original RO membrane by polyamide. The sharp peak at 1,684 cm^{-1} was assigned to aromatic ketones. They were formed by the oxidation of GA in an alkaline solution. The peak at 1,170 cm^{-1} belongs to the O═S═O group in the PSF membrane. The peaks at 1,658, 1,541, and 1,610 cm^{-1} were corresponding to the C═O (amide I) stretching vibration peak, the N–H (amide II) plane bending vibration peak in the amide bond, and the C═O (amide I) associated with hydrogen bonds of the stretching vibration peak (16,17). These characteristic absorption peaks of typical aromatic polyamides confirm the successful preparation of polyamide separation layers on PSF membranes (18).

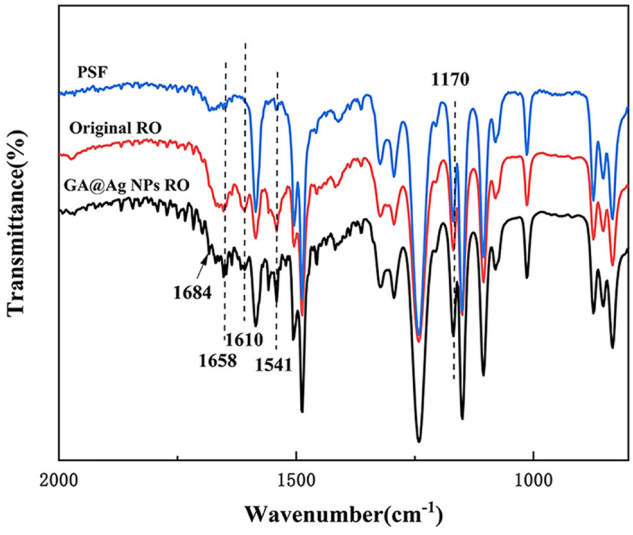

Figure 7: ATR-FTIR scanning pattern on the membrane surface.

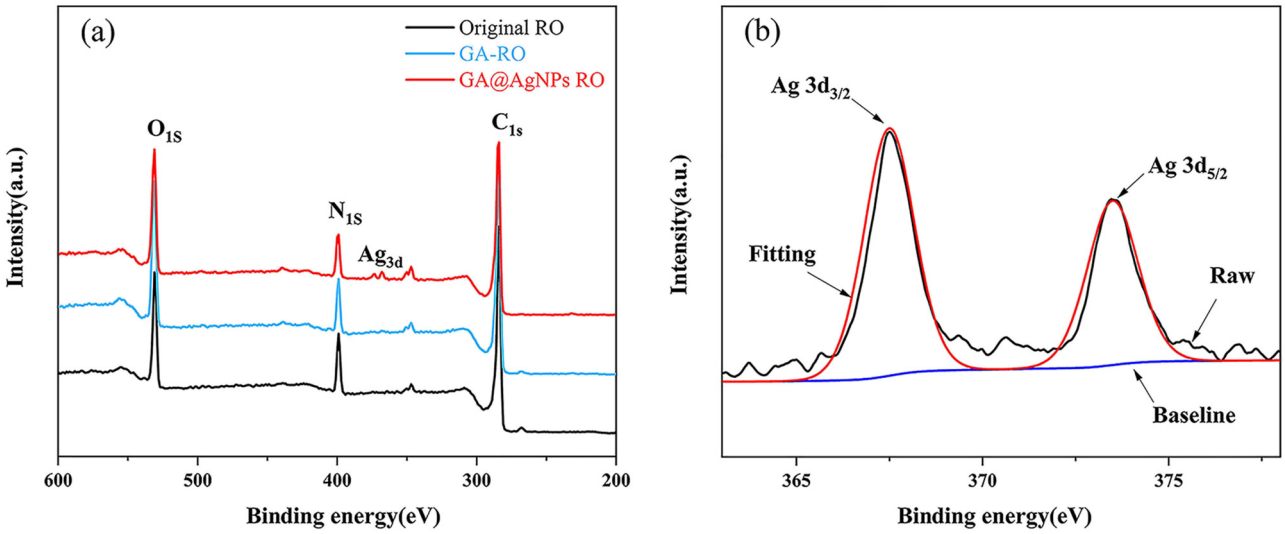

Figure 8: XPS spectra of the generated GA@AgNPs RO membranes (a) and the existence formation of Ag element (b).

The peaks at 1,658, 1,541, and 1,610 cm^{-1} were all slightly enhanced compared to the RO membrane by only polyamide, indicating increased amide bonds. Due to the amide reaction between the carboxyl group on the GA units and the amine group on the MPD units in the mixed water solution. Therefore, the FTIR results confirmed that GA was successfully connected to the GA@AgNPs RO membrane.

3.2.4 The existence of the formation of Ag element

The changes in the chemical composition of the surface of the generated RO membrane were calculated by XPS analysis. Figure 8a shows the full XPS spectra of the original RO membrane by polyamide (black curve), the GA-RO membrane (blue curve), and the generated GA@AgNPs RO membrane (red curve). Figure 8b shows the peak deconvolution of the narrow-scan XPS spectrum of the GA@AgNPs RO membrane.

It can be observed in Figure 8a that the spectra of these three samples were very similar. The spectrum of the GA@AgNPs RO membrane presented two new peaks of Ag $3d_{3/2}$ and Ag $3d_{5/2}$ with binding energies of 374 and 368 eV, respectively, which indicated the presence of silver atoms (19). It can be seen in Figure 8b that, except for Ag, almost no peaks of other chemical states exist in the spectrum, which further indicates the existence of the

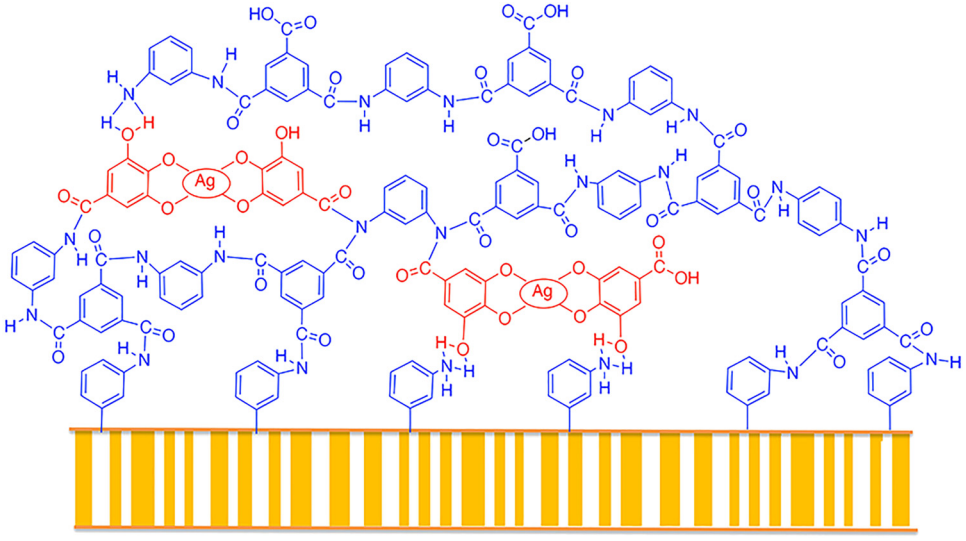

Figure 9: The structure model of the GA@AgNPs RO membrane.

formation of AgNPs on the membrane surface. Therefore, the results of the XPS analysis confirmed that AgNPs were successfully introduced onto the RO membrane.

3.2.5 The structure model of the generated GA@AgNPs RO membrane

Based on the results of SEM, AFM, FTIR, and XPS analysis and the chemical reactions principles, the structure model of the generated GA@AgNPs RO membrane can be established as shown in Figure 9.

3.3 The performance of the GA@AgNPs RO membrane

The water flux of the GA@AgNPs RO membrane was 31.1 $L \cdot m^{-2} \cdot h^{-1}$, which was 46.7% higher than that of the original membrane, which was prepared on the PSF basement membrane by adding a mixed solution with TEA, CAS, MPD, and TMC. The salt rejection rate by the GA@AgNPs RO membrane remained between 93.8% and 97.6%.

The reason for the increase of water flux through the GA@AgNPs membrane is as follows: on the one hand, the AFM analysis shows that the doping of GA@AgNPs increases the roughness of the membrane, thus increasing the contact area between the membrane and water molecules, which is conducive to the penetration of water molecules. On the other hand, some voids generated between the AgNPs and polyamide layers can provide additional nanochannels for the fast transport of water molecules, thereby enhancing the water flux of the membrane. Moreover, it has a strong inhibitory ability against microorganisms. The bacteriostatic rate of GA@AgNPs RO membrane against *E. coli* and *S. aureus* was above 99.9%, which was calculated based on the results of *E. coli* colonies and *S. aureus* colonies as shown in Figure 10.

There are four reasons for the strong antibacterial ability. First, the GA@AgNPs RO membrane contains AgNPs. Those AgNPs can attach to bacterial surfaces and penetrate into bacteria, thereby destroying living bacteria (20). Second, AgNPs can generate reactive oxygen species to disrupt DNA replication (21). Third, the toxicity of AgNPs can be driven by the release of silver ions, which can easily combine with the sulfhydryl groups on bacterial cell membranes, thereby inhibiting cellular enzyme activity (9,22).

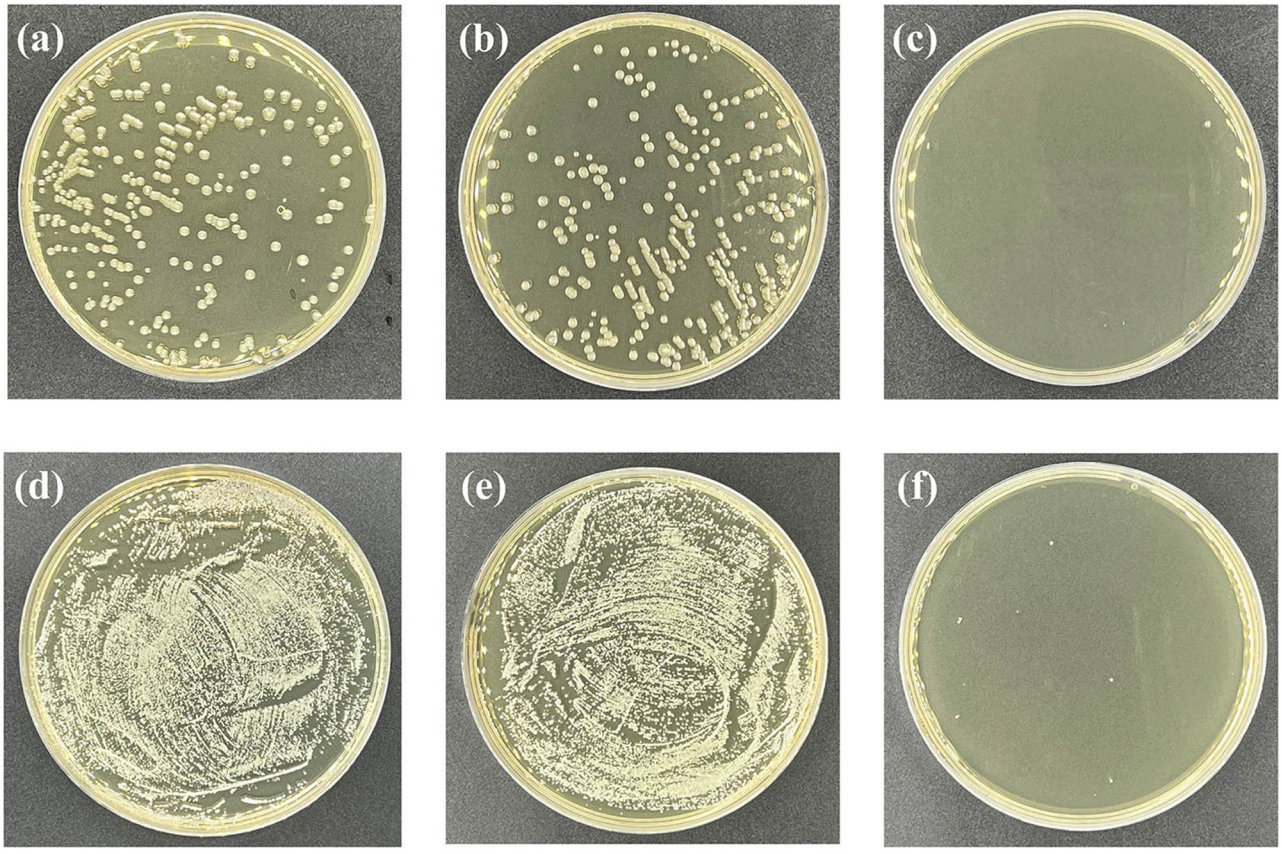

Figure 10: Photographs of the bacterial culture plates of *E. coli* (a–c) and *S. aureus* (d–f) for virgin (a and d), original RO membrane (b and e), and GA@AgNPs RO membrane (c and f).

Fourth, silver ions can activate oxygen molecules in air or water to generate hydroxyl radicals and superoxide radicals, which can further oxidize and kill bacteria without illumination (20).

3.4 The stability of GA@AgNPs RO membrane

The GA@AgNPs RO stability was analyzed using UV-Vis DRS. Figure 11 shows the UV-Vis diffuse reflection spectrum of the GA@AgNPs RO membrane at different time periods, which characterizes the light absorption properties of the GA@AgNPs RO membrane. As shown in Figure 11, the GA@AgNPs RO membrane has strong light absorption ability in the UV-Vis range, and the absorption edges are 271 nm. It can be seen from Figure 11 that the UV absorption peaks of the prepared GA@AgNPs RO membranes after being placed for 1, 5, 15, and 25 days have similar peak shapes and their half-peak widths basically do not change, indicating that the GA@AgNPs RO membranes have good stability.

3.5 Discussions on the reaction mechanisms of AgNPs generation

Based on the SEM and AFM images, it can be seen that there are many convex structures on the surface of the original RO membrane. Those raised structures were a typical feature of the active layer on the surface of the aromatic polyamide composite membrane via MPD and TMC as the monomers. However, when the original RO membrane touched a silver nitrogen solution, some of the raised structures drew back. As the amino groups on the polyamide units react with silver ions, the substances in the raised structures are agglomerated. Thus, it strongly affects the permeability and desalination rate of the RO membrane. Therefore, it indicated that directly applied silver ions to the original RO membrane were not proposed.

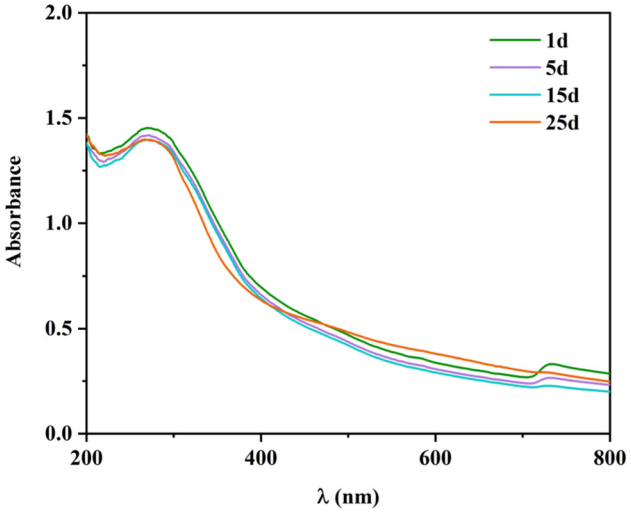

Figure 11: UV-Vis diffuse reflection spectrum of GA@AgNPs RO membrane at different time periods.

For this reason and based on the inspired by literature, we got an idea of using GA to react with silver nitrogen solution to generate a kind of stable AgNPs for the antibacterial property of the RO membrane. The reaction mechanisms can be explained as follows.

First, silver nitrogen dissociated into silver ions and nitrate anions. Then, dissociated silver ions were coordinated by the hydroxyl groups on GA molecules. As a result, it caused a decentralization of silver ions and avoided connecting silver ions directly to amino compounds to generate an agglomeration. The reactions can be expressed as follows:

$$AgNO_3 + H_2O \rightarrow Ag^+ + (NO_3^-) \quad (4)$$

$$Ag^+ + GA \rightarrow Ag^+GA \quad (5)$$

Second, the intermediate product of Ag^+GA was reduced to generate AgNPs by the reduction of MPD, which converted to *m*-dinitrobenzene (MD) (23–26). The reactions can be expressed as Eq. 6. By the way, AgNPs were successfully formed. The generated AgNPs were also coordinated by the hydroxyl groups on the GA molecules in the water solution, resulting in an even decentralization of the AgNPs. This judgment was supported by literature and the XPS characterization mentioned earlier.

$$Ag^+GA + MPD \rightarrow GAAg(NPs) + MD \quad (6)$$

3.6 Discussion on the advance and shortage of this research

A new type of RO membrane was successfully prepared by a simple method, and a high-quality RO membrane with higher permeability and higher antibacterial ability was obtained. In contrast, Yang et al. and Ben-Sasson et al. reduced silver ions using the strong reducing agent $NaBH_4$ (11,12). In this article, we focus on the multifunctional design of MPD, where the MPD monomer contains primary amine groups for forming the main polyamide network while also acting as a reducing agent for silver ions. Therefore, it provides a new idea for the reduction of

silver ions, avoiding the use of additional toxic reducing agents and bridging agents. We applied GA@AgNPs to the RO membrane and realized the uniform dispersion of AgNPs on the RO membrane. In addition, the GA@AgNPs RO membrane preparation method only needs to add modified materials based on the traditional RO preparation process. We synthesized an RO membrane with uniformly dispersed AgNPs in one step through interfacial polymerization, which improved the antibacterial and permeability properties of the RO membrane. Therefore, the developed method is simple and easy to industrialize.

Based on the results of SEM, AFM, FTIR, and XPS analyses, as well as the chemical structures of the generated products, we developed a structural model of the generated GA@AgNPs RO membrane and revealed the reaction mechanism of GA with silver nitrogen. This provides a scientific theory and technology for the preparation and dispersion of AgNPs that inhibits microorganisms in the membrane industry. However, our work does not explore the performance of the membranes in practical applications. Further studies are needed before GA@AgNPs RO membranes can be put on the market.

4 Conclusions

A novel GA@AgNPs RO membrane was fabricated by incorporating GA-modified AgNPs into the polyamide layer during interfacial polymerization. The doped GA-modified AgNPs can be uniformly dispersed on the membrane, and the roughness of the membrane is increased, so that the water flux of the membrane increases to 31.1 $L \cdot m^{-2} \cdot h^{-1}$, which is 46.7% higher than that of the original membrane. The rejection performance of the GA@AgNPs RO membrane was not affected, and the salt rejection rate remained at 93.8–97.6%. In addition, due to the intrinsic properties of AgNPs, the bactericidal activity of GA@AgNPs RO membrane was significantly enhanced, and the inhibition rate against both *E. coli* and *S. aureus* exceeded 99.9%.

Acknowledgement: The authors would like to thank the National Natural Science Foundation of China and the Guangxi Science and Technology Foundation for research funding.

Funding information: This project is supported by the National Natural Science Foundation of China (Grant No. 21868006) and the Guangxi Science and Technology Foundation (Grant No. AA17204067).

Author contributions: Zou Xiaofang: writing – original draft, writing – review and editing, methodology, visualization, formal analysis; Tian Zhu: formal analysis, methodology; Tang Jiangquan: formal analysis, methodology; Weixing Gan: project administration, funding acquisition; Guangzai Nong: project administration, writing – review and editing, formal analysis, visualization, methodology, supervision.

Conflict of interest: The authors state that there is no conflict of interest.

Data availability statement: All data generated or analyzed during this study are included in this published article.

References

(1) Misdan N, Lau WJ, Ismail AF. Seawater Reverse Osmosis (SWRO) desalination by thin-film composite membrane – Current development, challenges and future prospects. Desalination. 2012;287:287228–37. doi: 10.1016/j.desal.2011.11.001.

(2) Patel SK, Ritt CL, Deshmukh A, Wang Z, Qin M, Epsztein R, et al. The relative insignificance of advanced materials in enhancing the energy efficiency of desalination technologies. Energy Environ Sci. 2020;13(6):1694–710. doi: 10.1039/d0ee00341g.

(3) Huang X, Chen Y, Feng X, Hu X, Zhang Y, Liu L. Incorporation of oleic acid-modified Ag@ZnO core-shell nanoparticles into thin film composite membranes for enhanced antifouling and antibacterial properties. J Membr Sci. 2020;602:117956. doi: 10.1016/j.memsci.2020.117956.

(4) Matin A, Khan Z, Zaidi SMJ, Boyce MC. Biofouling in reverse osmosis membranes for seawater desalination: Phenomena and prevention. Desalination. 2011;281:2811–16. doi: 10.1016/j.desal.2011.06.063.

(5) Prihasto N, Liu Q-F, Kim S-H. Pre-treatment strategies for seawater desalination by reverse osmosis system. Desalination. 2009;249(1):308–16. doi: 10.1016/j.desal.2008.09.010.

(6) Kochkodan V, Hilal N. A comprehensive review on surface modified polymer membranes for biofouling mitigation. Desalination. 2015;356:356187–207. doi: 10.1016/j.desal.2014.09.015.

(7) Zhang C, Hu Z, Deng B. Silver nanoparticles in aquatic environments: Physiochemical behavior and antimicrobial mechanisms. Water Res. 2016;88:88403–27. doi: 10.1016/j.watres.2015.10.025.

(8) Shuai C, Guo W, Wu P, Yang W, Hu S, Xia Y, et al. A graphene oxide-Ag co-dispersing nanosystem: Dual synergistic effects on antibacterial activities and mechanical properties of polymer scaffolds. Chem Eng J. 2018;347:347322–33. doi: 10.1016/j.cej.2018.04.092.

(9) Chernousova S, Epple M. Silver as antibacterial agent: Ion, nanoparticle, and metal. Angew Chem Int Ed. 2013;52(6):1636–53. doi: 10.1002/anie.201205923.
(10) Yin J, Yang Y, Hu Z, Deng B. Attachment of silver nanoparticles (AgNPs) onto thin-film composite (TFC) membranes through covalent bonding to reduce membrane biofouling. J Membr Sci. 2013;441:44173–82. doi: 10.1016/j.memsci.2013.03.060.
(11) Ben-Sasson M, Lu X, Bar-Zeev E, Zodrow KR, Nejati S, Qi G, et al. In situ formation of silver nanoparticles on thin-film composite reverse osmosis membranes for biofouling mitigation. Water Res. 2014;62:62260–70. doi: 10.1016/j.watres.2014.05.049.
(12) Yang Z, Takagi R, Zhang XY, Yasui T, Zhang L, Matsuyama H. Engineering a dual-functional sulfonated polyelectrolyte-silver nanoparticle complex on a polyamide reverse osmosis membrane for robust biofouling mitigation. J Membr Sci. 2021;618:118757. doi: 10.1016/j.memsci.2020.118757.
(13) Kahkeshani N, Farzaei F, Fotouhi M, Alavi SS, Bahramsoltani R, Naseri R, et al. Pharmacological effects of gallic acid in health and diseases: A mechanistic review. Iran J Basic Med Sci. 2019;22(3):225–37. doi: 10.22038/ijbms.2019.32806.7897.
(14) Tamuly C, Hazarika M, Borah SC, Das MR, Boruah MP. In situ biosynthesis of Ag, Au and bimetallic nanoparticles using *Piper pedicellatum* C.DC: Green chemistry approach. Colloid Surf B. 2013;102:102627–34. doi: 10.1016/j.colsurfb.2012.09.007.
(15) Ramon GZ, Hoek EMV. Transport through composite membranes, part 2: Impacts of roughness on permeability and fouling. J Membr Sci. 2013;425-426:425141–8. doi: 10.1016/j.memsci.2012.08.004.
(16) Tang CYY, Kwon YN, Leckie JO. Effect of membrane chemistry and coating layer on physiochemical properties of thin film composite polyamide RO and NF membranes I. FTIR and XPS characterization of polyamide and coating layer chemistry. Desalination. 2009;242(1–3):149–67. doi: 10.1016/j.desal.2008.04.003.
(17) Zou H, Jin Y, Yang J, Dai HJ, Yu XL, Xu J. Synthesis and characterization of thin film composite reverse osmosis membranes via novel interfacial polymerization approach. Sep Purif Technol. 2010;72(3):256–62. doi: 10.1016/j.seppur.2010.01.019.
(18) Kang GD, Yu HJ, Liu ZN, Cao YM. Surface modification of a commercial thin film composite polyamide reverse osmosis membrane by carbodiimide-induced grafting with poly(ethylene glycol) derivatives. Desalination. 2011;275(1–3):252–9. doi: 10.1016/j.desal.2011.03.007.
(19) Huang LC, Zhao S, Wang Z, Wu JH, Wang JX, Wang SC. In situ immobilization of silver nanoparticles for improving permeability, antifouling and anti-bacterial properties of ultrafiltration membrane. J Membr Sci. 2016;499:499269–81. doi: 10.1016/j.memsci.2015.10.055.
(20) Kedziora A, Speruda M, Krzyzewska E, Rybka J, Lukowiak A, Bugla-Ploskonska G. Similarities and differences between silver ions and silver in nanoforms as antibacterial agents. Int J Mol Sci. 2018;19(2):444. doi: 10.3390/ijms19020444.
(21) Duran N, Duran M, De Jesus MB, Seabra AB, Favaro WJ, Nakazato G. Silver nanoparticles: A new view on mechanistic aspects on antimicrobial activity. Nanomed Nanotechnol. 2016;12(3):789–99. doi: 10.1016/j.nano.2015.11.016.
(22) Sambhy V, Macbride MM, Peterson BR, Sen A. Silver bromide nanoparticle/polymer composites: Dual action tunable antimicrobial materials. J Am Chem Soc. 2006;128(30):9798–808. doi: 10.1021/ja061442z.
(23) Tian J, Luo Y, Li H, Lu W, Chang G, Qin X, et al. Ag@poly(m-phenylenediamine)-Ag core-shell nanoparticles: one-step preparation, characterization, and their application for H_2O_2 detection. Catal Sci Technol. 2011;1(8):1393–8. doi: 10.1039/c1cy00212k.
(24) Zhang YW, Wang L, Tian JQ, Li HL, Luo YL, Sun XP. Ag@Poly(m-phenylenediamine) core-shell nanoparticles for highly selective, multiplex nucleic acid detection. Langmuir. 2011;27(6):2170–5. doi: 10.1021/la105092f.
(25) He Y, Huang L, Zhao Y, Yang W, Hao T, Wu B, et al. A newly synthesized highly stable Ag/N-carbon electrode for enhanced desalination by capacitive deionization. Environ Sci Nano. 2020;7(10):3007–19. doi: 10.1039/d0en00826e.
(26) Zhang L, Chai L, Liu J, Wang H, Yu W, Sang P. pH Manipulation: A facile method for lowering oxidation state and keeping good yield of poly(m-phenylenediamine) and its powerful Ag^+ adsorption ability. Langmuir. 2011;27(22):13729–38. doi: 10.1021/la203162y.